Journal of Environment and Earth Science
ISSN 2224-3216 (Paper) ISSN 2225-0948 (Online)
Vol.5, No.9, 2015
www.iiste.org

Physicochemical Characterization of Lomo Black Shale and Application as Low Cost Material for Phosphate Adsorption in Aqueous Solution

Lassina Sandotin Coulibaly*
Université de Lorraine, CNRS, GeoRessources UMR 7359,
Rue du Doyen Roubault, B.P. 40, 54501 Vandœuvre-lès-Nancy, France
Université Nangui abrogoua, Laboratoire Géosciences et Environnement (LGE),
02 B.P. 802 Abidjan 02, Côte d'Ivoire

Jacques Yvon
Université de Lorraine, CNRS, CREGU, GeoRessources laboratory,
Rue du Doyen Marcel Roubault, B.P. 40, 54501 Vandoeuvre-les-Nancy, FRANCE

Lacina Coulibaly,
Université Nangui Abrogua, Laboratoire Environnement et Biologie Aquatique (LEBA),
Abidjan, 02 B.P. 802 Abidjan 02, Côte d'Ivoire

Abstract
The characterization of shale powder fraction from Lomo Nord (Ivory Coast) was performed in order to find potential applications for this material as phosphate low-cost adsorbents. The crushed shale (ø < 80µm) consisted of quartz, albite, microcline, chlorite, dolomite and kaolinite as associated minerals. The net effective charge of shale particle, determined using microelectrophoresis, is shown to be negative for all pH values. Batch experiments were performed with phosphate synthetic water to study the adsorption equilibrium and influence of contact time, adsorbent dosage, initial concentration, temperature and pH on the phosphate adsorption onto the shale. Kinetic data revealed that more than 0.046 mg/g of phosphate was adsorbed onto shale within 10 hours. The maximum phosphate adsorption capacity of the shale powder was 0.32 mg/g. The dependency of the phosphate sorption capacity with the pH is clearly evidenced. Shale achieved the maximum removal of phosphate (70 %) over the pH range 4 – 10. Thermodynamic tests indicate that phosphate sorption to shale increased with temperature (from 20 to 40°C), indicating the spontaneous and endothermic nature of sorption process ($\Delta H°$ = 8.22 kj/mol, $\Delta S°$ = 0.015 kj/mol, $\Delta G°$ = 3.52 - 3.82 kj/mol). $\Delta G°$ values shows dominance of physisorption process. But, the results indicate that the pseudo second order model was most suitable for describing the kinetic data, revealing that some chemical interaction also occur. The Freundlich, Langmuir and Dubinin-Radushkevich models were used to simulate the sorption equilibrium. The Freundlich model showed more applicability than others. These finding demonstrate that Lomo shale's could be used as an efficient low-coast adsorbent to remove phosphate from water.
Keywords: Phosphate, adsorption, isotherms, kinetics, shale, thermodynamics.

1. Introduction

Phosphorus is often present in relatively large amounts in water bodies, which are especially close to human activities. Such presence is explained by the fact that wastewater plants and agriculture runoff are their main source. Phosphorus and ammonium are essential nutrients for the growth of aquatic plants and algae in ecosystems, and therefore are a major cause of eutrophication. As environmental concern, eutrophication may deteriorate the water quality and damage the balance of organism. Some previous works presented phosphorus as the limiting factor that could stop eutrophication (Bourdon *et al.* 2004). Hence, it is necessary to decrease the concentration of phosphate in wastewater before its discharge. Several methods have been applied to remove efficiently and rapidly phosphates, including precipitation–microfiltration (Lu & Liu 2010), reverse osmosis (Zhao & Sengupta 1998; Badruzzaman & Oppenheimer 2007), coagulation (Tchobanoglous *et al.* 2003; Yeom *et al.* 2008) and adsorption (Vohla *et al.* 2011; Brogowski & Renman 2004; Karaca *et al.* 2004; Bellier *et al.* 2006). Chemical or electrochemical precipitation, both pose a significant problem in terms of disposal of the precipitated wastes and ion-exchange treatments do not appear to be economical. Among these methods, adsorption has attracted more attention due to its high efficiency, easy regeneration and reuse of adsorbents, and economical advantages. Several material or by-products were used as adsorbent by different researchers (Drizo *et al.* 1999; Johansson & Gustafson 2000; Cheung & Venkitachalam 2000; Huang & Chriswell 2000; Codling *et al.* 2000; li *et al.* 2006). From these works, the general trend worldwide is to develop cheap adsorbent from locally available materials.

The black shale investigated here as adsorbent is a natural geological material available in large

amount in Ivory Coast. It is a dark-colored mud rock containing organic matter, silt and clay minerals grains that accumulated together.

The first objective of this study was to determine the shale mineralogical and textural characteristics, major chemistry and surface properties that might play a role in adsorption. The second objective was to assess the feasibility of using shale powder for the removal of phosphate from synthetic aqueous solutions. In addition, kinetics and isotherms models were used for data fitting.

2. Material and methods

2.1. Material

2.1.1. Shale

The shale used in this research is local natural material collected at Lomo Nord, in Ivory Coast (Center). It was washed several times to remove earthy matter and finally rinsed with distilled water. Then, the samples were crushed and sieved to have a desired particles size (less than 80 µm) using a Saulas NF.X 11.501 sieve. It was directly used as an adsorbent without any additional treatment.

2.1.2. Adsorbate

An artificial phosphate solution with pure K_2HPO_4 was used to make the sorption tests. Hydrogeno phosphate was used for his solubility at low temperature (20°C) in water and it ability to produce reactive phosphate ions (PO_4^{3-}, HPO_4^{2-}, H_2PO^{4-}). The reactive inorganic orthophosphate ions are the forms generally found in wastewater in where phosphate is most readily available for biological utilization (**Nesbitt 1986**) and thus contribute to the eutrophication of water bodies. A stock solution of 150 mg/L of phosphate was prepared by dissolving chemically pure K_2HPO_4 in distilled water. The pH value of the phosphate solution was adjusted to 6.0-7.0 with diluted HCl and NaOH before adsorption experiments.

2.2. Experimental methods

2.2.1. Physical and textural properties

2.2.1.1. Particle size distribution

Particle size distribution was determinate using a Helos Sympactec type apparatus. For this purposes 1 g of shale sample was introduced in a 50 ml of 0.1% (w/w) $(NaPO_3)_6$ solution. Prior to the particle size analyses, the shale powder suspension was dispersed by ultrasound for 2 min.

2.2.1.2. Cation exchange capacity (CEC)

The cation exchange capacity (CEC) was measured by cobalt-hexammonium ions permutation (Mantin and Glaeser 1960). The amount of cobalt-hexammonium ions fixed by the solid phase was determined by UV-vis spectroscopy. The displaced cations were also determined by atomic absorption spectrometry using a Perkin-Elmer 1100B apparatus.

2.2.1.3. Specific surface areas and total pore volume

Specific surface areas and pore size distributions for shale powder sample were obtained from N_2 adsorption/ desorption isotherms at 77K after outgazing at 105°C and 10^{-3} Torr. Isotherms were recorded on a step-by-step automatic home built set up. Specific surface areas (SSA) were determined from adsorption data according to the Brunauer-Emmet-Teller (BET) equation and using 16.3$Å^2$ for the cross section area of nitrogen. The error in the determination of the SSA was estimated as +/- 1 m^2/g. Micropores volumes and non microporous surface areas were obtained using the t-plot method proposed by DeBoer et *al.* (1996). Pore size distributions were calculated on the desorption branch using the Barrett-Joyner-Halenda (BJH) method, assuming slit-shaped pores (Delon & Dellyes 1967).

2.2.2. Mineralogical analyses

2.2.2.1. Morphology and chemical analysis

Morphology is studied by Scanning electron microscopy (SEM) method. The analysis was performed on polished thin sections after carbon coating, using a Hitashi FEG S 4800 device equipped with an Energy Dispersive X-ray Spectrometer (EDS) and a back scattered secondary electrons detector. The elementary composition was determined using inductive coupled plasma atomic emission spectrometry (ICP-AES) for major elements. Before analyses, the sample was fused in lithium borate ($LiBO_2$) and the obtained glass dissolve using nitric acid.

2.2.2.2. X-ray diffraction study

X-ray diffraction (XRD) data were obtained by reflection on powdered material, using a diffractometer BRUKER D8 advance employing CoKα radiation (1.789Å) radiation at 40 kV and 30 Ma. It was used to identify the mineralogical phases of the shale.

2.2.2.3. FTIR Spectroscopy

Fourier transform infrared spectroscopy was carried on in diffuse reflection mode (DRIFTS), using a Bruker Equinox 55 instrument. The spectra were recorded from 4000 cm^{-1} to 600 cm^{-1} with a resolution of 4 cm^{-1} on KBr powder containing 15 % of shale powder.

2.2.3. Surface charges measurement

The Zero Point Charge of Lomo shale particles was obtained by electrophoresis mobility method using a CAD Instrumentation Zetaphoremeter III model Z3000. The measurements were performed at room temperature using a shale suspension (60 ± 5 mg/L) in an electrolytic background of $NaClO_4$ (10^{-1}, 10^{-2} and 10^{-3} M). The pH was adjusted between 3 and 11 by adding aliquots of dilute HCl or NaOH solution.

2.2.4. Adsorption experiments

Phosphate adsorption experiments were undertaken in the batch equilibrium technique. An aliquot of the stock solution prepared below was diluted in deionized water to prepare the desired experimental concentrations.

The phosphate removals as a function of dosage were conducted at an initial P concentration of 5 mg/L with a wide range of adsorbent masses of 0,1-10 g in 50 ml of solution. The solutions were shaken at 180 rpm. After 48h, samples were centrifuged (Sorval rc Evolution centrifugal machine) at 21859 g for 30 min, then, the supernatants were filtered through a 0.45 µm membrane filter. The filtrate was taken for phosphate analysis in a double beam UV-VIS spectrophotometer (Shimadzu, 2051 PC) at 450 nm using the ammonium molybdate method (Blanchet et Malaprade 1967). The optimum dose was then determined and used throughout all adsorption experiments.

The effect of pH on phosphate adsorption was examined in a series of experiments using the initial phosphate concentration of 5 mg/L at pH 2, 4, 6, 8 or 10. The acidic or alkaline pH was controlled by adding the required amounts of dilute hydrochloric acid (HCl) or sodium hydroxide (NaOH) solutions. The pH of the sample was determined using a pH meter (Meter Lab, Model PHM 210). The solutions were stirred during 24 h and then, the concentration of phosphate in the solution was measured.

Phosphate sorption kinetics was evaluated at three initial concentrations (2.5; 5; 10 mg/L) at 303.15 K. The initial phosphate concentrations were selected in reference to concentrations in typical effluent waters (Tchobanoglous *et al.* 2003). Before each kinetic experiment, a given amount of adsorbent was put in conical flasks 50 ml. Then 50 ml of initial phosphate solution was added. The flask was covered and immediately placed in a thermostatic chamber with magnetic stirring. The pH was maintained between 6 and 7 and, if necessary, adjusted by using 0.1 M NaOH or 0.1 M HCl solution. This pH values are also typical of water effluents. The test solution was sampled with syringes (40 ml) after various reactions times (0 to 24h) and the samples were collected for phosphate concentration measurement. The additional experiments were performed at 20, 30 and 40°C to examine the isotherms and the effect of temperature on phosphate adsorption. To implement each equilibrium adsorption isotherm, the adsorbent was added to 50 ml of different levels of initial artificial phosphate solutions (0; 1; 2.5; 5; 10; 25; 50; 100 ;150 mgP/L). The mixture were capped in order to minimize losses to atmosphere, and stirred at 180 rpm for 6 hours. The pH was maintained between 6 and 7 and, if necessary, adjusted as below. After a reaction period, the mixtures were centrifuged and the residual phosphate concentrations were measured.

All of the batch experiments were performed in triplicate and only average values are presented. The percentage adsorbed (r %), and the phosphate adsorption capacity of shale (q) were calculated using the relation (1) and (2) respectively :

$$r\,[\%] = \frac{(C_o - C)}{C_o} \times 100 \qquad (1)$$

$$q = \frac{(C_o - C)_x V}{m} \qquad (2)$$

Where C_o (mg/L) is the initial phosphate concentration, C (mg/L) is the phosphate concentration at the time t, V (L) is the volume of solution and m (g) is the mass of shale powder in solution.

2.3. Adsorption modeling

2.3.1. Adsorption kinetic

The phosphate adsorption mechanism from an aqueous solution by shale could be explained using kinetic models and examining the rate-controlling mechanism of the adsorption process. These models provide information about the dynamics of the adsorption process in terms of the order and the rate constant which are of significance in designing and modeling an efficient adsorption operation. First-order, pseudo-second-order, Elovich and Weber's intraparticle diffusion models are the kinetic models used here (Ho & McKay 1998; Karaca *et al.* 2004; Feng *et al.* 2009).

The first-order rate equation is as follows:

$$\frac{dq_t}{dt} = k_1(q_e - q_t) \qquad (3)$$

The pseudo-second-order model equation is given as:

$$\frac{dq_t}{dt} = k_2(q_e - q_t)^2 \quad (4)$$

The Elovich model can be expressed as:

$$\frac{dq_t}{dt} = \alpha\, exp(-\lambda q_t) \quad (5)$$

Where q_e and q_t are respectively the amounts of phosphate (mg/g) adsorbed onto adsorbent at equilibrium and at time t, k_1 and k_2 are the first-order and second-order constants (h^{-1}) respectively, α (mg/g. min) is the initial adsorption rate constant and the parameter β (g/mg) is related to the extent of the surface coverage and activation energy for chemisorption.

For the same boundary conditions (at t = 0, $q_t = 0$ and at t = t, $q_t = q_t$), the integrated form of the pseudo first order, the pseudo second order and the Elovich model become respectively:

$$\ln(q_e - q_t) = \ln q_e - k_1 t \quad (6)$$

$$\frac{t}{q_t} = \frac{t}{q_e} + \frac{1}{k_2 q_e^2} * t \quad (7)$$

$$q_t = \frac{1}{\lambda} * \ln(\lambda\beta) + \frac{1}{\lambda}\ln(t) \quad (8)$$

The Weber's intraparticle diffusion model (**Weber et Morris 1963**) can be expressed by the following equation:

$$q_t = k_d t^{1/2} + C \quad (9)$$

Where *C* is the intercept and k_d is the intraparticle diffusion rate constant (mg/g $h^{1/2}$).

2.3.2. Adsorption isotherm

Adsorption is usually described through isotherms, that is, the amount of phosphate adsorbed on shale as a function of its equilibrium concentration at constant temperature. The quantity adsorbed is nearly always normalized by the mass of shale to optimize the design of an adsorption system and to allow comparison with other materials. The Langmuir, Freundlich and Dubinin–Radushkevich isotherms are the most common models used to describe the equilibrium adsorbed phosphate (q_e) and phosphate in solution (C_e) at a given temperature.

The Langmuir theory has, as its basic assumption, that adsorption occurs at specific homogeneous sites inside of the adsorbent and, once an adsorbates molecule occupies a site, no additional adsorption can occur there (Langmuir, 1916). The saturated monolayer curve can be represented by the expression:

$$q_e = \frac{q_{max} k_L c_e}{1 + k_L c_e} \quad (10)$$

The Freundlich isotherm model is considered to be appropriate for describing both multilayer sorption and sorption on heterogeneous surfaces with interaction between adsorbed molecules (Weber 1963). The Freundlich equation may be written as:

$$q_e = k_F C_e^n \quad (11)$$

Dubinin–Radushkevich (D-R) isotherm model predicts the mechanism of the adsorbate sorption onto the adsorbent, and it is used to calculate the mean free energy of adsorption (Singh & Pant 2004). The nonlinear D–R isotherm is expressed as:

$$q_e = q_m Exp\ (-\beta.\varepsilon^2) \quad (12)$$

Where q_e is the amount of solute adsorbed per mass of adsorbent (mg/g), qm is the maximum adsorption capacity (mg/g), b is the D–R constant (mol^2/J^2) and ε is the Polanyi potential (J/mol), which can be calculated as:

$$\varepsilon = RT\left(1 + \frac{1}{C_e}\right) \quad (13)$$

Where R is the gas constant (J/mol K), T is the absolute temperature (K), and C_e is the equilibrium concentration of the adsorbate in aqueous solution (mg/L). The mean free energy of adsorption (*E*) was calculated from the β values using the following equation (Singh & Pant 2004):

$$E = \frac{1}{\sqrt{2\beta}} \quad (14)$$

The *E* value is used to ascertain the type of adsorption process under consideration. If this value is between 8 and 16 kJ/mol, the adsorption process can be assumed to involve chemical sorption. On the other hand, values lower than 8 kJ/mol indicate that the adsorption process is of a physical nature.

2.3.3. Thermodynamic

The experimental data obtained as a function of different temperatures were analyzed to determine the thermodynamic parameters as change in the Gibbs free energy (ΔG°), enthalpy (ΔH°) and entropy (ΔS°) that evaluate the thermodynamic feasibility and the nature of the adsorption process. The following equations were used:

$$\Delta G^\circ = \Delta H^\circ - T\Delta S^\circ \quad (15)$$

$$\Delta G^\circ = -RTlnk_d \qquad (16)$$

$$\ln k_d = \frac{\Delta S^\circ}{R} - \frac{\Delta H^\circ}{RT} \qquad (17)$$

$$k_d = \frac{q_e}{C_e} \qquad (18)$$

Where R is the gas constant (8.314 J/mol/K), T is the temperature (K) and k_d is the equilibrium constant (dimensionless) reflecting the phosphate distribution between the solid (q_e) and liquid phases at equilibrium (C_e). The values of (ΔH°) and (ΔS°) were determined by plotting ln k_d versus 1/T using equation (17) and the value of ΔG° was calculated from Equation (15).

2.3.4. Error analysis

To ascertain the model that best described phosphate adsorption the least squares regression (R) analysis was used. Although efficient, this indicator is limited to solving models that present linear forms (Wong *et al.* 2004). Therefore, in this work, Chi-square analysis was also performed to compare the experimental data with model predictions in accordance with Leiviskä *et al.* (2013):

$$\chi^2 = \sum \frac{(q_e - q_{e,m})^2}{q_{em}} \qquad (19)$$

Where q_e is the equilibrium capacity (mg/g) from the experimental data and $q_{e,m}$ the equilibrium capacity obtained with a model (mg/g). If the calculated values of Chi-square are smaller than the critical value at 5% level of probability, the model data are similar to the experimental data.

3. Results and discussion

3.1. Black Shale properties or Characterization

3.1.1. Particle size distribution

The shale powder was sieved to obtain a particle size lower than 80 µm. The particle size distribution of the shale powder is given in Figure 1. One could observe that 83% of the total amount of particles had sizes between 0.05 and 40 µm, with a maximum at 5.8 µm.

3.1.2. Structural Property of prepared black shale

The N_2 adsorption desorption isotherms and pore sizes distribution curve are presented in Figure 2. The isotherms shows increased N_2 adsorption at low relative pressures (P/Po < 0.02), which is indicative of microporosity. The hysteresis observed at higher relative pressures ($P/P_0 > 0.5$) indicated the presence of some mesopores or micropores in the shale minerals (Gregg & Sing 1982). The V_t (total volume), A_{meso} (mesopore equivalent area), and A_{micro} (micropore area) of shale powder are 3.8 cm^3/g, 13 m^2/g and 4.1m^2/g respectively. Furthermore, the specific surface area determined by t-plot method was calculated to be 16.8 m^2/g. Which was higher than the BET specific surface area (16.5 m^2/g), therefore, this difference also indicated that the shale sample was porous. These results reveal that porosity is developed for shale and mainly exists in the form of micropores as shown in Figure 2a.

3.1.3. Scanning electron microscopy of crushed shale

Figure 3 illustrates the SEM micrograph of a typical natural crushed rock. The shale particles were mostly irregular in shape and appeared to have randomly arranged pores framework (Figure 3a), which is expected to enhance adsorption through particle diffusion. These observations confirm that the material is porous as shown previously. It is also observed that shale particles are not homogeneous and contained separated crystals. The EDS analysis reveals that the clear crystals with a size of about 20 µm (Figure 3b) are apatite. The small white crystals (size of about 5 µm) which are shown with black arrows could be attributed to monazite. The phyllitic minerals appearing as sticks (see white circle) are mostly chlorite containing magnesium (Figure 3a).

3.1.4. Chemical composition

The chemical compositions of shale sample are given in Table 1. The most abundant oxide is SiO_2 (55.43 %). Al_2O_3 and Fe_2O_3 content (9.21–15.46 %) were slightly higher than the others oxides, whereas, K_2O, CaO, Na_2O, MgO, TiO_2, MnO and P_2O_5 are present only in small quantities. Similar results were obtained by Kabran (1988). The P_2O_5 (0.56%) and CaO (2.34%) content can be related to the presence of minor amounts of apatite and monazite. The relative high content of MgO (2.92), Na_2O (2.09) and K_2O (3.13) are likely due to the presence of Na/K-feldspath and magnesian chlorite.

3.1.5. Mineralogical analyses and Cation Exchange Capacity

The powder XRD pattern of the black shale is illustrated in Figure 4. According to the reflection values, shale includes quartz (4.25, 3.34, 2.46, 2.28, 2.23, 2.12 and 1.82 Å), Albite (6.36, 4.02, 3.77, 3.60, 3.21, 3.19 and 2.92

Å), Microcline (6.46, 3.29, 3.24 and 2.16 Å), chlorite (14.38, 7.20, 4.81, 4.58 and 3.60 Å) kaolinite (7.20, 3.60 and 2.46 Å) and dolomite (2.89 Å). The predominant mineral of the studied sample is quartz, its amount in this material agrees with the results obtained by Martin (1977) and Monde *et al.* (2008).

FTIR analysis of shale was undertaken and the spectrum is presented in Figure 5. Position and assignment of vibrational bands of this black shale are shown in Table 2 (Schroeder 2002; Farmer 1974; Igisu *et al.* 2006; Saikia *et al.* 2008). This technique confirmed the presence of minerals already observed by XRD. In addition, the presence of two other minerals has been revealed. In fact, the bands at 744, 727 and 609 cm^{-1} reflects the bending of Si–O bonds of albite. Apatite mineral are detected by bending bands of PO_4 at 604 cm^{-1}.

Table 3 shows the CEC of shale sample, as can be seen, the CEC values is about 33.1 mEq/100g. For cations exchanged, the following order is privileged: Sodium, calcium and then magnesium and potassium showing the great influence of feldpath. On the other hand, the low CEC obtained in comparison with those reported in literature is due to the presence of considerable amount of non-clay minerals as quartz and likely the absence of smectite clay.

3.1.6. Surface charges

The Figure 6 presents zeta potentials of the shale in the pH range from 3 to 11. It can be seen that the electrophoretic mobility values increase in absolute value from -1.23 to -2.83 µm/s/v/cm with increasing of pH. The electrophoretic mobility is related to the particle electric charge. For particle having a permanent charge, the variation of the mobility with pH is rather low (Tombácz & Szekeres 2006). Hence, the low dependency of the mobility *vs.* pH is indicative of the existence of a permanent charge. This permanent charge is confirmed through the split of the curves to lower mobility value with the increase of the ionic force. However, the pH dependency is indicative of a variable charge that is probably due to protonation-deprotonation of edges surface functions. These results indicate that the net surface charge is negative and would not change to positive regardless of pH. So, the ZPC of a variable-charged particle in solution which is defined as the pH where, the zeta potential or the net total charge of moving particle is zero, is never reached. The absence of the ZPC, usual for permanently charged particles, confirmed that the shale particles have a permanent negative charge. Therefore, the decrease of electrophoretic mobility values indicates that the screening of the shale particles charge is poor at high pH because of the presence of negatively charge hydroxyl groups. Consequently, it possible to predict that, theoretically phosphate adsorption onto shale will increase by lowering the pH of initial phosphate solution. The pH lowering will favor the screening of the particles negative charge which results in a reduction of electrostatic repulsion between the phosphate ions and the shale particles.

3.2. Adsorption experiments

3.2.1. Phosphate adsorption characteristics (Influence of adsorbent mass, optimal contact time, initial concentration and temperature effects)

The characteristics of phosphate sorption to shale that include the effects of adsorbent mass, contact time, initial concentration and temperature were investigated (Figure 7). The effect of the amount of shale dosage on the removal of phosphate is shown in Figure 7a. As it can be seen, the percent removal increased with increasing adsorbent dosage, probably due to the increase amount of the adsorbent surface. At the adsorbent dosage of 100 g/L the maximum adsorption efficiency is reached at about 75%. When the dosage is increased beyond 100 g/L, a decrease in the percentage of adsorption is observed which may result from the electrostatic interactions, interference between binding sites, and reduced mixing at higher adsorbent contents (Çoruh & Geyikçi 2012). In this study, 100 g/L would be the optimum mass dosage of shale particles.

In order to establish the equilibrium time for maximum uptake and to know the kinetics of adsorption process, the phosphate removal by shale was investigated as a function of contact time for 24 h using three different initials concentrations 2.5, 5 and 10 mg/L. It was observed from Figure 7b that the curves are of saturation type and the chemical equilibrium is attained after a short reaction time. In fact, after the initial rapid reaction less than 30 min, phosphate sorption continued to proceed at a slow rate within the range of ½ h to 24 h and the state of dynamic equilibrium between the phosphates desorption and adsorption is reached before 24 h. The fast adsorption rate at the initial stage quantitatively predominant may be explained by an increased availability in the number of active binding sites on the adsorbent surface. In the second stage, the slower adsorption rate is probably due to the gradual occupancy of these binding sites, the adsorption of the exterior surface reached saturation, herein, the sorption is likely an attachment-controlled process due to less available sorption sites. This latter phenomenon takes a relatively long contact time. The adsorption of phosphate reached equilibrium at variable time according to the initial concentration of phosphate: about 1, 10 and 14 h for initial phosphate concentration of 2.5, 5 and 10 mg/L respectively. At the same equilibrium times, the amount of phosphate adsorbed range from 0.023 to 0.072 mg/g. The higher the initial concentration of phosphate species, the larger is the amount of phosphate species adsorbed. This is a result of the increase in the driving force and the concentration gradient, as an increase in the initial phosphate concentrations, because the resistance to the phosphate uptake decreased as the mass transfer driving force increased. As seen, the phosphate adsorption

capacity strongly depends on the initial P concentration of solution.

The phosphate equilibrium sorption at 20, 30 and 40°C onto shale was also studied. An increase in the temperature led to an increase in the adsorption capacity as shown in Figure 7c. Several factors may account for the increase in sorption with increasing temperature. Increased diffusion rate of adsorbates molecules across the external boundary layer and in the internal pores of shale particle, owing to the decrease in the velocity of the solution may account for the observed behavior (Wang & Zhu 2007). Changes in the adsorbent pore sizes as well as an increase in the number of sorption sites due to the breaking of some internal bonds near the edges of the particle are expected at higher temperatures (Yadava *et al.* 1988; Low *et al.* 1997). An increase in temperature may also affect an increase in proportion and activity of phosphate ions in solution, the affinity of the ions for the surface, or the charge and therefore the potential of the shale surface (Barrow 1990 and 1992).

3.2.2. Influence of pH

The effect of the phosphate solution pH on phosphate removal was studied in the pH range from 2 to 12. The experimental data are illustrated in Figure 8. As shown on mineralogical composition, shale contain phosphate mineral as apatite and monazite, so the negative value of efficiency between pH 2 and 2,5 is certainly due to the dissolution of these phosphate minerals that increase the amount of phosphate species in solution. Furthermore, phosphate species at low pH chiefly existed in the form of phosphoric acid, which would restrict the adsorption of PO_4^{3-} onto shale and lead to a low adsorption capacity (Li *et al.* 2006). When the pH is increased beyond 2.5, both, the adsorption phenomena became more important than the dissolution phenomena and phosphate species are less in acid form. Therefore, one could observe the positive value of phosphate retention efficiency. At pH 4 the sorption efficiency reaches 75 % and the removal remains relatively constant up to pH 10, whereas phosphate removal decreased sharply as the solution pH approaches highly alkaline condition (pH 12). The decrease of adsorption capacity at pH > 10 can be attributed to the competition between hydroxyl ions and phosphates ions for adsorption sites. It could also be explained based on sorbent surface charge. In fact, on the basis of electrophoretic mobility studies, the global net charge of shale surface is negative. Nevertheless, at high pH, the shale surface negatives sites (unfavorable for phosphate adsorption) are more predominant than when the pH is low. These results clearly indicate that the adsorption of phosphate onto shale strongly depends on pH value. The convenient pH for optimal adsorption are found to lie between 4 and 10.

3.2.3. Adsorption kinetic, isotherm and thermodynamic analyses

3.2.3.1. Adsorption kinetic

In order to examine the mechanism of adsorption and potential rate-controlling step, such as mass transfer and chemical reaction processes, the experimental data obtained as a function of the reaction time were analyzed using the pseudo first-order, pseudo second-order, Elovich and intraparticle kinetic models (Figure 9). The constant parameters of the kinetics equation and the correlation coefficients values are summarized in Table 4. The correlation coefficients (R) of all examined kinetic data with the pseudo second order model were found very high (R > 0.99) it is indicated that the model is more appropriate to be used for adsorption process of phosphate. Meanwhile, *q* values determined by pseudo-second-order model were in perfect agreement with the experimental results. This concordance confirms that the pseudo second- order model can be effectively used to predict the adsorption kinetic of phosphate by shale. The good agreement with pseudo-second-order model demonstrated that the adsorption determining step may be the valence forces through sharing or exchange of electrons between the adsorbent and the adsorbate (Anirudhan *et al.* 2012). The adsorption data cannot be described entirely by intraparticle diffusion model; however, as shown in Figure 9d, the plots present multi-linearity which can inform about adsorption process. For 10 mg/L of phosphate initial concentrations, plot show three steps. The first step was ascribed to the diffusion of phosphate from the external solution to the external surface of shale or instantaneous adsorption stage. The second step was the intraparticle diffusion. The intraparticle diffusion slowed down and reached equilibrium during the third stage. The plot corresponding to the initial phosphate concentration of 5 mg/L show two steps, herein, intraparticle diffusion is not occurring due to the low concentration of phosphate. For the 2.5 mg/L of phosphate initial concentrations, only the equilibrium step is observed resulting from the fast rate of the instantaneous step. Equilibrium is certainly reached before the first sampling. This observation is consistent with the k_2 values found. One could also, observe that plots did not pass through the origin, indicating that the diffusion is not the rate limiting step. Furthermore, adsorption process on shale may be of complex nature consisting of both surface adsorption and intra-particle diffusion.

3.2.3.2. Isotherms analyses

In order to find the most suitable isotherm model for representing the experimental data, the adsorption data were fitted with the Freundlich, Langmuir and Dubinin-Radushkevich isotherm models. The results are shown in Figure 10. The isotherms parameters obtained in fitting experimental data, with the correlation coefficients and Chi-square values at different temperatures are summarized in Table 5 and 6.

The coefficient of correlation (R > 0,983) and the lowest value of the Chi-square analysis ($\chi^2 < 0,03$) indicate that the Freundlich isotherm was suitable for describing the equilibrium data. In the case of good adsorption characteristics, n_F is between 2 and 10 (Leiviskä *et al.* 2013). The n_F obtained values (2.07, 1.78,

1.70) (Table 5) lies within this range indicating that the adsorption of phosphate onto the shale is favorable in the studied conditions. The maximum adsorption capacity (q_m) was calculated with k_F and 1/n at different temperatures. The value of q_m was calculated to be 0.39, 0.33 and 0.23 mg/L which are in the range of phosphate adsorption capacity reported in literature (Drizo *et al.* 1999; Heal *et al.* 2003; 2005, Xu *et al.* 2006; Prochaska & Zouboulis 2006)(Table 7).

3.2.3.3. Thermodynamic parameters of the adsorption of phosphate onto shale

The thermodynamic analysis for phosphate sorption to shale powder is presented in Figure 11. The thermodynamic parameters are provided in Table 8. The positive value of ΔH° (8.22 Kj/mol) confirms the endothermic nature of phosphate sorption. The positive value of ΔS° (0.015 KJ/mol.) indicates that the randomness increased at the interface between solid and solution during the sorption process. The Gibbs free energy (ΔG°) indicates the degree of spontaneity of the sorption process. The ΔG° values are positive at different temperatures, revealing that the adsorption process of phosphate onto shale is not spontaneous. Moreover, decrease in value of ΔG◦ from 3.82 to 3.52 with change in temperature from 20 to 40°C suggests that higher temperature is favorable to the adsorption. So if the temperature is higher enough the spontaneity of the reaction will occur. Generally, ΔG° values between - 20 kJ/mol and 0 kJ/mol suggests a physisorption process, whilst ΔG° values in range of - 80 kJ/mol to - 400 kJ/mol suggest a chemisorption process (Atkins 1990). One could observe that the ΔG° values in Table 8 are neither within the ranges of ΔG° in physisorption nor chemisorption process; however, they seem more close to the values of ΔG° values in a physisorption process. It is likely that in addition to physisorption, some other mechanisms may be involved, i.e. electrostatic interactions and ligands exchange.

4. Conclusion

After mineralogical, physico-chemical and surface properties studies, the black shale from Ivory Coast was investigated as an adsorbent for the removal of phosphate from aqueous solution. It appears that black shale consist of varying minerals such as quartz, Albite, Microcline, chlorite, apatite, dolomite and clay minerals as kaolinite. The chemical composition reveal high amount of SiO_2 (55.43%), Al_2O_3 (15.46 %) and Fe_2O_3 (9.21 %), with minor amounts of K_2O, CaO, Na_2O, MgO, TiO_2, MnO and P_2O_5. The SEM micrographs reveal the morphological heterogeneity of shale and flat particles with well-defined shape and a size of approximately 5 to 20 µm. They also suggest macroporous-mesoporous network. This observation is confirmed by textural results that indicate that the porosity mainly exists in the form of micropores. The developed SSA is about 16.5 m^2/g. Results also indicate that the net surface charge is negative and would not change regardless of pH. The adsorption study revealed that the process depended significantly on contact time, initial phosphate concentration, temperature and solution pH. The phosphate adsorption capacity increased with both the increasing initial phosphate concentration and the contact time, but equilibrium is reached after an agitation time of 10 hours. Based on the adsorption isotherm studies the uptake capacity of phosphate on shale at 40°C is larger than that at 30 and 20°C that show endothermic nature of adsorption. Furthermore, the adsorption kinetic of phosphate on the shale was better described by the pseudo-second-order because of the best correlation with experimental data. This last result and thermodynamic analyses indicated that phosphate adsorption onto shale is likely governed by both chemical and physical interactions. Freundlich, Langmuir and Dubinin-Radushkevich models have been used to test and correlate experimental data. Among, the three models used, the equilibrium isotherms were well described by Freundlich model. This study demonstrated that Lomo-nord black shale can be used as low cost-effective adsorbent for removing phosphate from wastewater.

References

Aksu, Z. & Kabasakal, E. (2004). Batch adsorption of 2,4-dichlorophenoxy-acetic acid (2,4-D) from aqueous solution by granular activated carbon. Separation and Purification Technology, 35, 223–240.

Anirudhan, T. S., Suchithra, P. S., Senan, P. & Tharun, A. R. (2012) Kinetic and equilibrium profiles of adsorptive recovery of thorium (IV) from aqueous solutions using poly(methacrylic acid) grafted cellulose/bentonite superabsorbent composite. *Indian Engineering Chemical Research,* 51, 4825–4836.

Atkins, P.W. (1990). *Physical Chemistry*. Oxford University Press, London, p 938.

Badruzzaman, M., Adham S. & Oppenheimer, J. (2007). Beneficial phosphate recovery from reverse osmosis (RO) concentrate of an integrated membrane system using polymeric ligand exchanger (PLE). *Water Research,* 41, 2211 – 2219.

Barrow, N. J. (1990). Relating chemical processes to management systems. Proceedings of Phosphorus requirements for sustainable agriculture in Asia and Oceania; March 1999, 199 – 209.

Barrow, N.J. (1992). A brief discussion on the effect of temperature on the reaction of inorganic ions with soil. *Journal of Soil Sciences* 43, (1) 37–45.

Bellier, N., Chazarenc, F. & Comeau, Y. (2006). Phosphorus removal from wastewater by mineral apatite. *Water Research,* 40, 2965 – 2971.

Bourdon, C., Choubert, J. M., Comeau, Y. & Héduit, A. (2004). Toward the Use of the BAP Test to Predict the Performance of Enhanced Biological Phosphorus Removal in Municipal WWTP, Ottawa, 29 October, University of Ottawa and Carleton University, p 77.
Brogowski, Z. & Renman, G. (2004). Characterization of opoka as a basis for its use in wastewater treatment. *Polish Journal of Environmental Studies,* 13 (1), 15 – 20.
Cheung, K. C. & Venkitachalam, T. H. (2000). Improving phosphate removal of sand infiltration system using alkaline fly ash. *Chemosphere* 41 : 243 – 249.
Codling, E. E., Chaney, R. L. & Mulchi, C. L. (2000). Use of aluminum and iron-rich residues to immobilize phosphorus in poultry litter and litter-amended soils. *Journal of Environmental Quality,* 29, 1924 – 1931.
Çoruh, S. & Geyikçi, F. (2012). Adsorption of copper (II) ions on montmorillonite and sepiolite clays : equilibrium and kinetic studies. *Desalination and Water Treatment*, 45, (1-3), 351 – 360.
De Boer, J. H., Linsen, B. G. & Osinga, T. J. (1996). Studies on pore systems in catalysts-Part VI : The universeal curve. *Journal of catalysis,* 4, 643–648.
Delon, J. F. & Dellyes, R. (1967). Calcul du spectre de porosité des minéraux phylliteux. C.R. Acad SC. Paris, 270 série D, 1661-1664.
Drizo, A., Frost, C. A., Grace, J. & Smith, K. A. (1999). Physico-chemical screening of phosphate removing substrates for use in constructed wetland systems. *Water Research,* 33 (17), 3595 – 3602.
Farmer, V. C. (1974). In the spectra of minerals. Edited by V.C. Farmer, 331p.
Feng-Chin, W., Ru-Ling, T. & Ruey-Shin, J. (2009). Characteristics of Elovich equation used for the analysis of adsorption kinetics in dye-chitosan systems. *Chemical Engineering Journal,* 150, 366 – 373.
Heal, K. V., Younger, P. L., Smith K. A., Glendinning S., Quinn P. & Dobbie K. E. (2003) Novel use of ochre from mine water treatment plants to reduce point and diffuse phosphorus pollution. *Land Contamination & Reclamation,* 11, 145–152.
Ho, Y. S. & McKay G., (1998). Sorption of dye from aqueous solution by peat. *Chemical Engineering Journal,* 70 (2), 115 – 124.
Huang, S. H. & Chiswell B. (2000). Phosphate removal from wastewater using spent alum sludge. *Water Science and Technology,* 42 (3–4), 295 – 300.
Igisu, M., Nakashima, S., Ueno, Y., Stanley, M., Awramiks, S. M. & Maruyama, S. (2006). In Situ Infrared Microspectroscopy of 850 Million-Year-Old Prokaryotic Fossils. *Applied Spectroscopy,* 60 (10), 1111 – 1121.
Johansson, L. (1999) Blast furnace slag as phosphorus sorbents column studies. *Science of The Total Environment*, 229, 89 – 97.
Kabran, P. K. B. (1988) "Pétrographie et géochimie des formations précambriennes de la région d'Odienné (Nord-Ouest de la Côte d'Ivoire). Typologie du volcanisme birimien - tendances évolutives du magmatisme Eburnéen - Géochimie de l'Uranium et du Thorium dans les granitoïdes". *PhD Thesis,* Sciences naturelles, Université d'Abidjan.
Karaca, S., Gürses, A., Ejder, M. & Açikyildiz, M. (2004). Kinetic modeling of liquid-phase adsorption of phosphate on dolomite. *Journal of colloid and interface Science,* 277, 257 – 263.
Langmuir I (1916) The constitution and fundamental properties of solids and liquids. *J Am Chem Soc* 38:2221–2295.
Leiviskä, T., Sarpola, A., Heikkinen, E. & Tanskanen, J. (2013). Thermal properties and phosphate adsorption efficiency of coarse aluminum silicate fraction. *Desalination and Water Treatment,* 51, (34-36), 6837– 6845.
Li, Y., Liu, C., Luan, Z., Peng, X., Zhu, C., Chen, Z., Zhang, Z., Fan, J. & Jia, Z. (2006). Phosphate removal from aqueous solutions using raw and activated red mud and fly ash. *Journal of Hazardous Materials* B137, 374–383.
Low, K. S., Lee, C. K. & Tan, S. G. (1997). Sorption of Trivalent Chromium from Tannery Waste by Moss. *Environmental Technology* 18 (4), 449– 454.
Lu, N. C. & Liu, J. C. (2010). Removal of phosphate and fluoride from wastewater by a hybrid precipitation–microfiltration process. *Separation and Purification Technology,* 74, 329–335.
Mantin, I. & Glaezer, R. (1960). Fixation des ions cobalti-hexamines par les motmorillonites acides. Bulletin du Groupe Français des Argiles 50, 83-88.
Martin L. (1977). "Morphologie, sedimentologie et paléogéographie au quaternaire récent du plateau continental ivoirien. " *PhD Thesis* Université de Paris VI.
Monde, S., Affian, K., Amani, E. M., Wognin, V. A., Coulibaly, A. S. & Aka, K. (2007) Analyse temporelle de l'hydrodynamisme du secteur estuarien de la lagune Ebrié à Abidjan (Côte d'Ivoire). Impact de la variabilité climatique. *Revue CAMES – Série A* (Sciences et Médecine), (5), 32 – 38.
Nesbitt, J. B. (1986). Phosphorus removal-the state of the art. *Journal (Water Pollution Control Federation),* 41, 701–713.
Prochaska, C. A. & Zouboulis, A. I. (2006). Removal of phosphates by pilot vertical-flow constructed wetlands using a mixture of sand and dolomite as substrate. *Ecological Engineering,* 26:293–303.

Saikia, B. J., Parthasarathy, G. & Sarmah N. C. (2008). Fourier transform infrared spectroscopic estimation of crystallinity in SiO2 based rocks. *Indian Academy of Sciences. Bulletin of Material Science*, 31 (5), 775 – 779.
Schroeder, P. A. (2002). Infrared Spectroscopy in clay science: In CMS Workshop Lectures, Vol. 11, Teaching Clay Science, A. Rule and S. Guggenheim, eds. *The Clay Mineral Society*, 11, 181– 206.
Semra, Ç. & Feza, G. (2012). Adsorption of copper (II) ions on montmorillonite and sepiolite clays: equilibrium and kinetic studies. *Desalination and Water Treatment*, 45, (1-3), 351-360.
Singh, T. S. & Pant, K. K. (2004). Equilibrium, kinetics and thermodynamic studies for adsorption of As (III) on activated alumina. *Separation and Purification Technology,* 36, 139 – 147.
Tchobanoglous, G., Burton, F. L. & Stensel, H. D. (2003). Wastewater engineering treatment and reuse. (4th ed/Rev). New York : Metcalf and Eddy.
Tombácz, E. & Szekeres, M., (2006). Surface charge heterogeneity of kaolinite in aqueous suspension in comparison with montmorillonite. *Applied Clay Science*, 34, 105-124.
Tourtelot, H. A. (1979). Black shale: Its deposition and diagenesis 1. *Clays and Clay Minerals*, 5, (27), 313 – 321.
Vohla, C., Koiva, M., Bavorb, H. J., Chazarenc, F. & Manderaet, U. (2011). Filter materials for phosphorus removal from wastewater in treatment wetlands - A review. *Ecological Engineering,* 37, 70 – 89.
Wang, S. & Zhu, Z. H. (2007). Humic acid adsorption on fly ash and its derived unburned carbon. *Journal of Colloid and Interface Science,* 315, 41– 46.
Weber, W. J. & Morris, J. C. (1963). Kinetics of adsorption on carbon from solution. *Journal of the Sanitary Engineering Division,* 89, 31 – 60.
Wong, Y. C., Szeto, Y. S., Cheung, W. H. & McKay G. (2004). Adsorption of Acid dyes on Chitosan, Equilibrium isotherm analyses. *Process Biochemistry,* 39 (6), 695–704.
Xu, D. F., Xu, J. M., Wu, J. J. & Muhammad, A (2006). Studies on the phosphorus sorption capacity of substrates used in constructed wetland systems. *Chemosphere,* 63, 344–352.
Yadava, K. P., Tyagi, B. S. & Singh, V. N. (1988). Removal of arsenic (III) from aqueous solution by china clay. *Environmental Technolology,* 11, 1233–1244.
Yeoman, S., Stephenson, T., Lester, J. N. & Perry, R. (1988). The removal of phosphorus during wastewater treatment: a review. *Environmental Pollution, 49*, 183–233.
Zhao, D. & Sengupta, A. K. (1998) Ultimate Removal and Recovery of Phosphate from Wastewater Using A New Class of Polymeric Exchangers. *Water Research,* 5(32), 1613–1625.

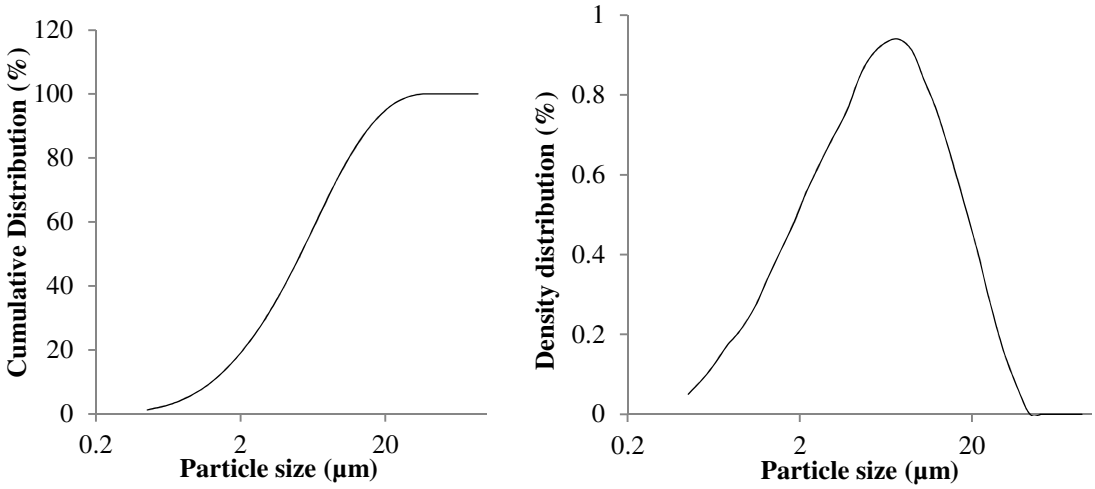

Figure 1. Particle size distribution by laser diffraction.

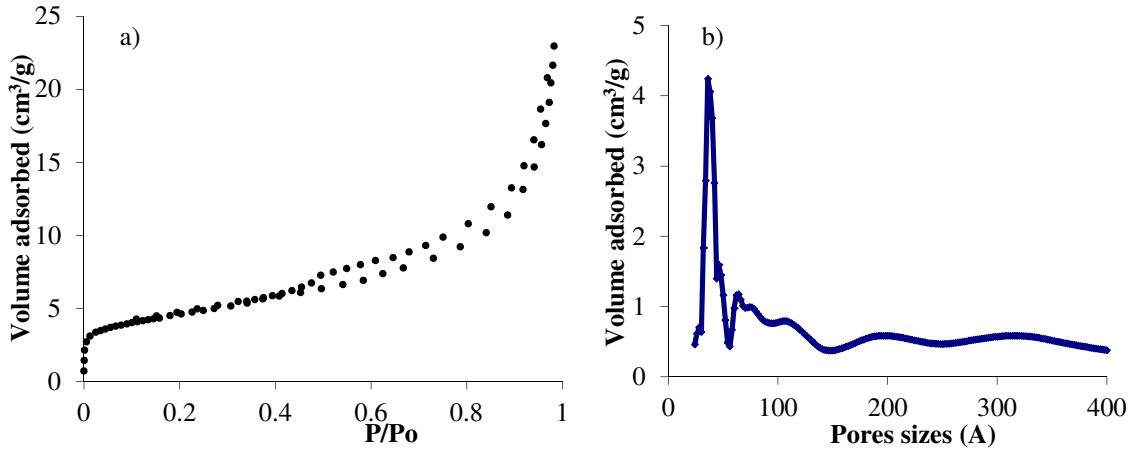

Figure 2. Nitrogen adsorption-desorption isotherms of the black shale (a) and pore size distribution obtained in terms of BJH method (b).

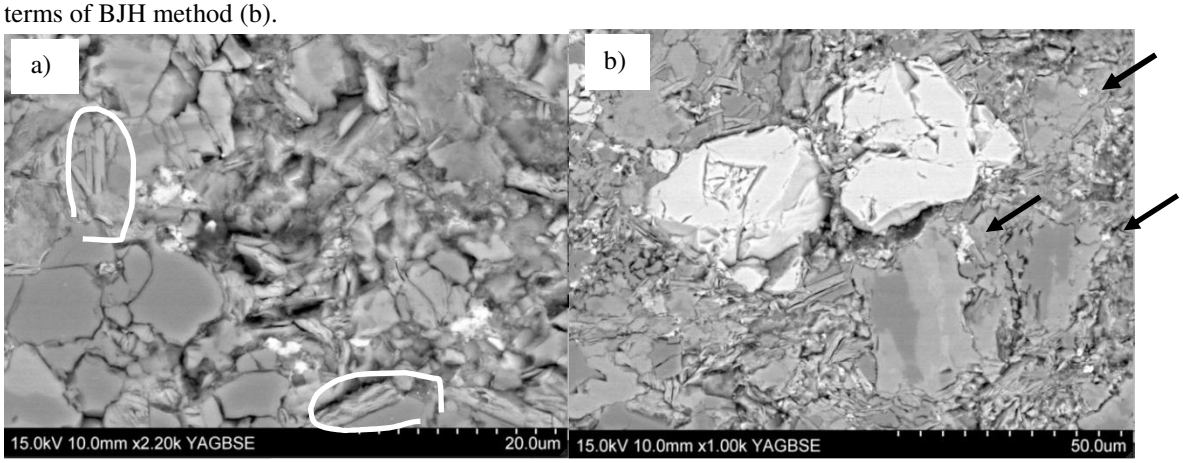

Figure 3. Scanning electron microscope micrographs of Lomo nord black shale

Table 1. Chemical composition (wt %) of the shale

Majors elements	SiO_2	Al_2O_3	Fe_2O_3	MnO	MgO	CaO	Na_2O	K_2O	TiO_2	P_2O_5	L.O.I.
wt %	55.43	15.46	9.21	0.29	2.92	2.34	2.09	3.13	1.01	0.56	7.52

L.O.I = Loss on ignition

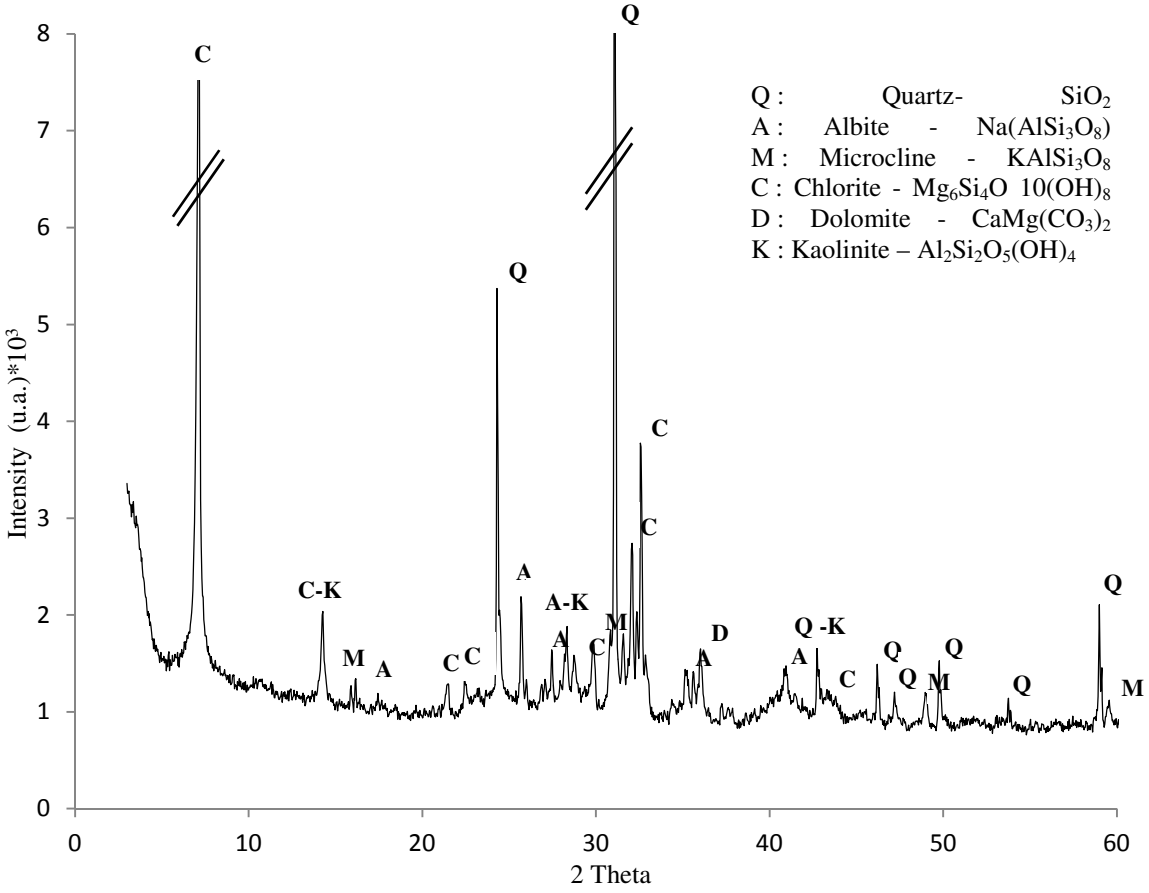

Figure 4. X-ray diffraction patterns of Lomo-Nord black shale

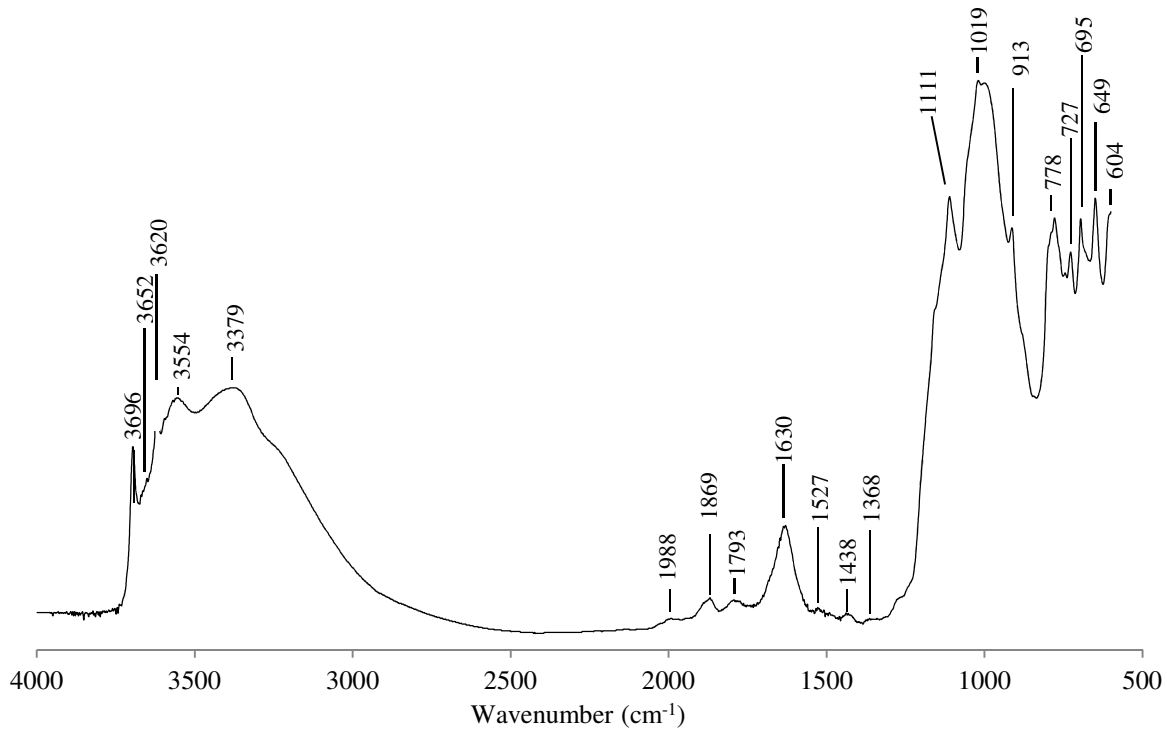

Figure 5. FTIR spectrum of Lomo-nord black shale

Table 2. FTIR band assignments of Lomo-nord black shale

Maxima (cm^{-1})	Assignments
3696 ; 3652 et 3620	-OH stretching, disordered kaolinite
3596 ; 3554	-OH stretching, chlorite
3379	-OH stretching, gibbsite
1988 ; 1869 ; 1793 ; 1527 ; 1111	-Si-O stretching and its harmonic, quartz
1630	-OH bending, hydratation
1438 ; 1368	carbonates
1019	-OH stretching, kaolinite
913	-δOH (internal) bending, Kaolinite
778 ; 695	Quartz
744 ; 727 ; 649	-Si-O bending, albite
604	-PO_4 bending, apatite

Table 3. Cation Exchange Capacity of Lomo nord black shale

Cations (mg/L)						CEC (mEq/100g)
Na^+	K^+	Ca^{2+}	Mg^{2+}	Fe^{2+}	Al^{3+}	33.13
13.04	6.4	85.9	11.2	0	0	

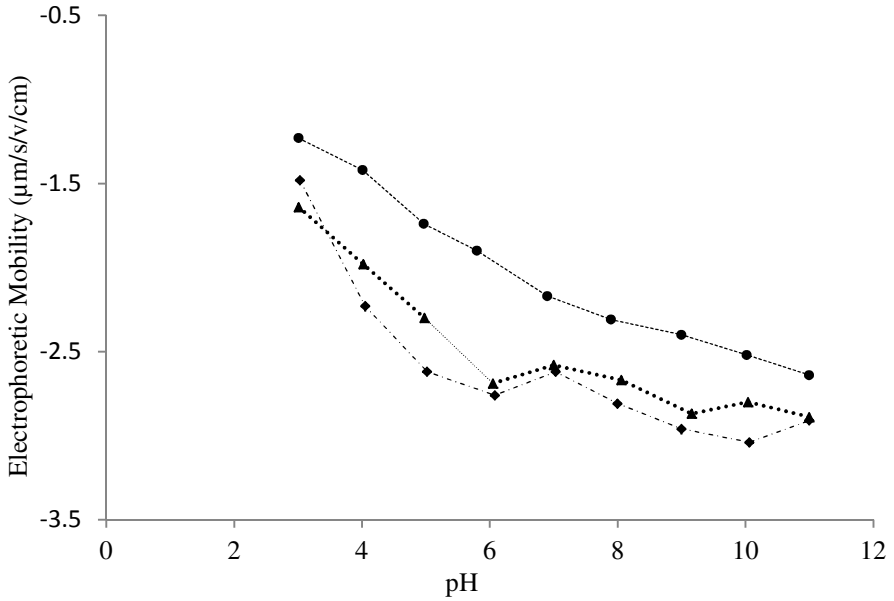

Figure 6. Electrophoretic mobility measurements on the shale: 10^{-1} M, 10^{-2}M and 10^{-3} M $NaClO_4$ solution.

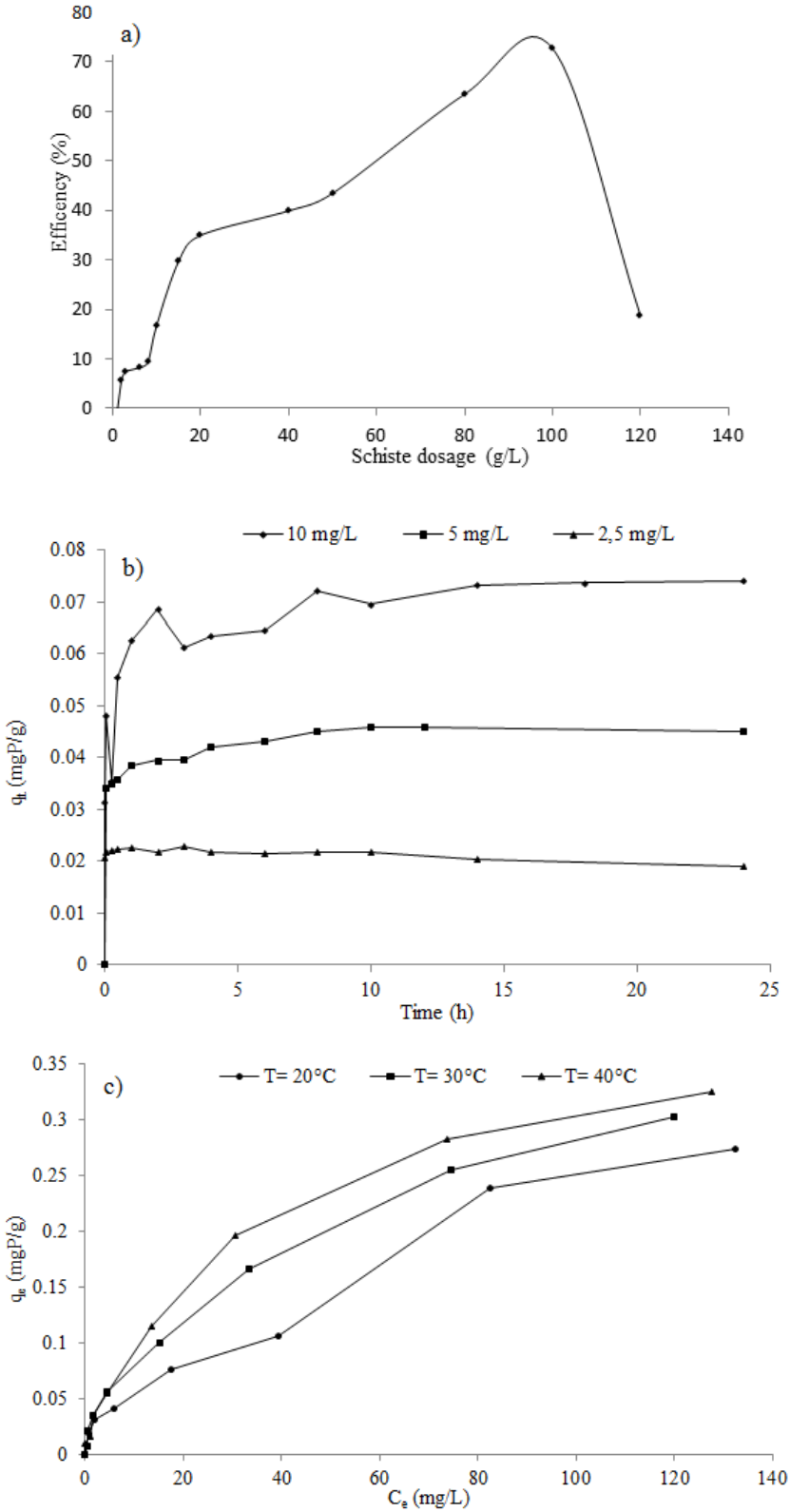

Figure 7. Phosphate adsorption on shale: (a) effect of adsorbent dosage (Initial P concentration 5 mg/L, at 30°C, pH = 6.5±0.5, agitation time: 24h.) (b) Effect of reaction time and initial phosphate concentration (Initial P concentration 2.5, 5 and 10 mg/L, at 30°C, pH = 6.5 ± 0.5, agitation time: 24h) and (c) effect of temperature (20, 30 and 40°C pH = 6.5 ± 0.5, agitation time : 10 h)

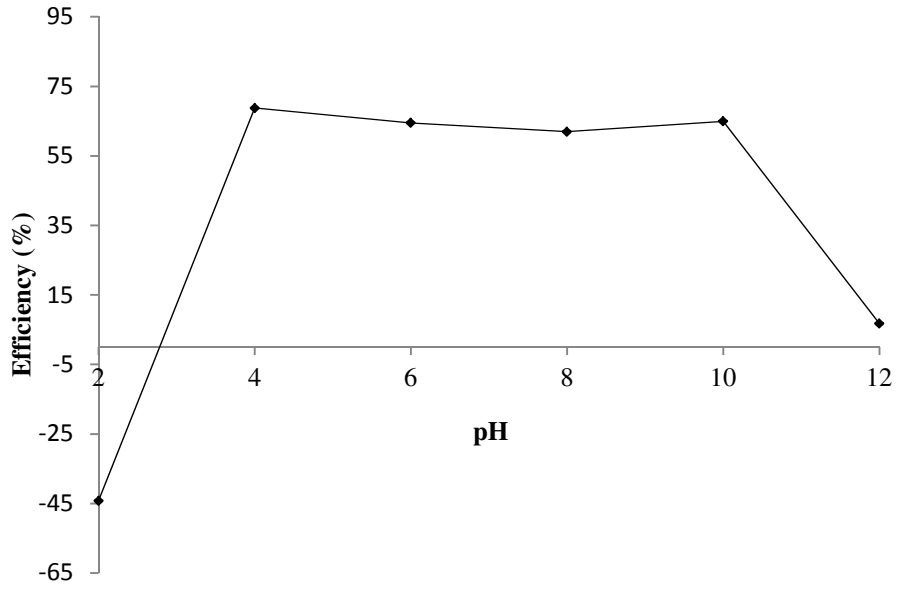

Figure 8. Phosphate removal as a function of pH. (Reactions conditions: Initial P concentration 5 mg/L, at 30°C, agitation time: 24h)

Table 4. Kinetic model parameters obtained from model fitting to experimental data.

C_o (mg/L)	$q_{e,\ exp}$ (mg/g)	Pseudo first order model			Pseudo second order model			
		$q_{e\ cal}$ (mg/g)	$k_1(h^{-1})$	R	$q_{e\ cal}$ (mg/g)	k_2	h $(mg.g^{-1}h^{-1})$	R
2.5	0.022	8.3_x10^{-4}	3_x10^{-3}	$8,3_x10^{-3}$	0.023	5290.66	4.567	0.99
5	0.046	0.013	0.245	0.98	0.046	114.39	4.1919	0,99
10	0.069	0.024	0.221	0.80	0.074	39.47	0.3707	0.99

C_o (mg/L)	Elovich model			Intraparticle diffusion models		
	α (mg/g.h)	β (g/mg)	R	k_d $(mg/h^{1/2}g)$	C	R
2.5	ND	105	0,26	2×10^{-5}	0.0219	0.62
5	12.7 x 103	0.0454	0,93	0.0074	0.0454	0.92
10	91.04	169.5	0,96	0.0074	0.0454	0.82

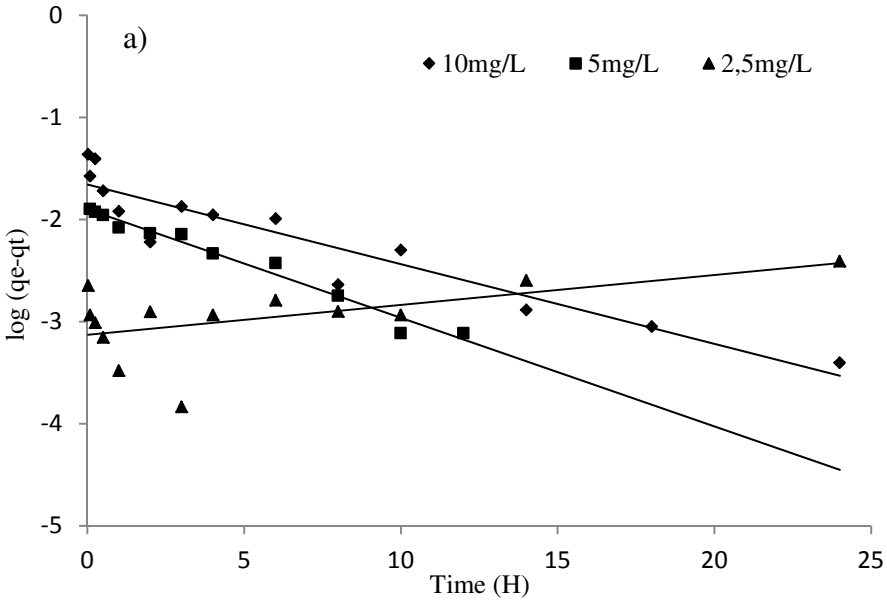
a)
10mg/L
5mg/L
2,5mg/L
log (qe-qt)
Time (H)

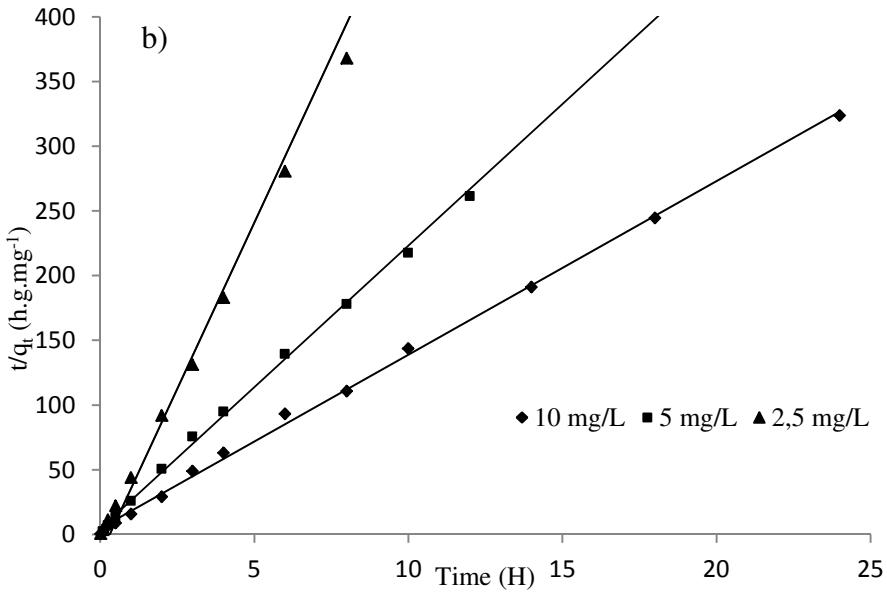
b)
10 mg/L
5 mg/L
2,5 mg/L
t/qt (h.g.mg-1)
Time (H)

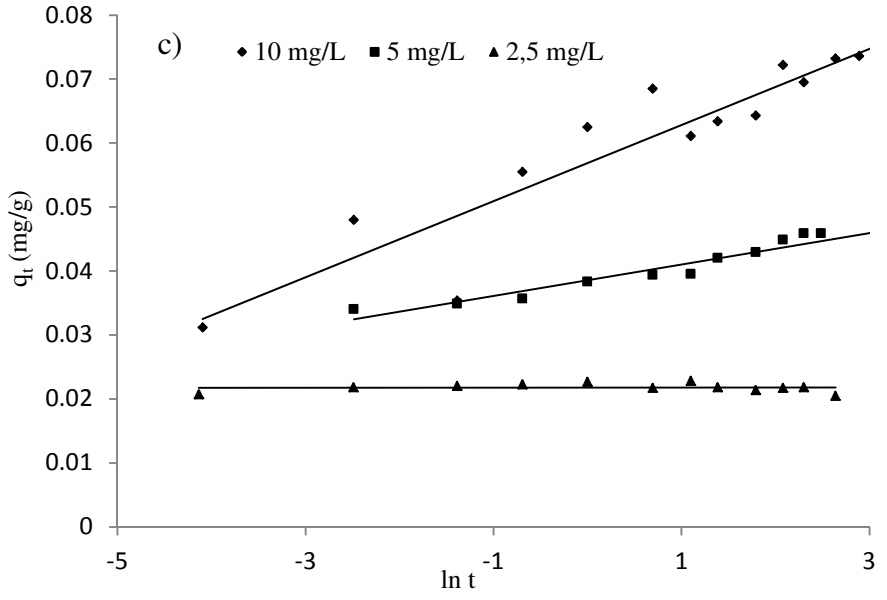
c)
10 mg/L
5 mg/L
2,5 mg/L
qt (mg/g)
ln t

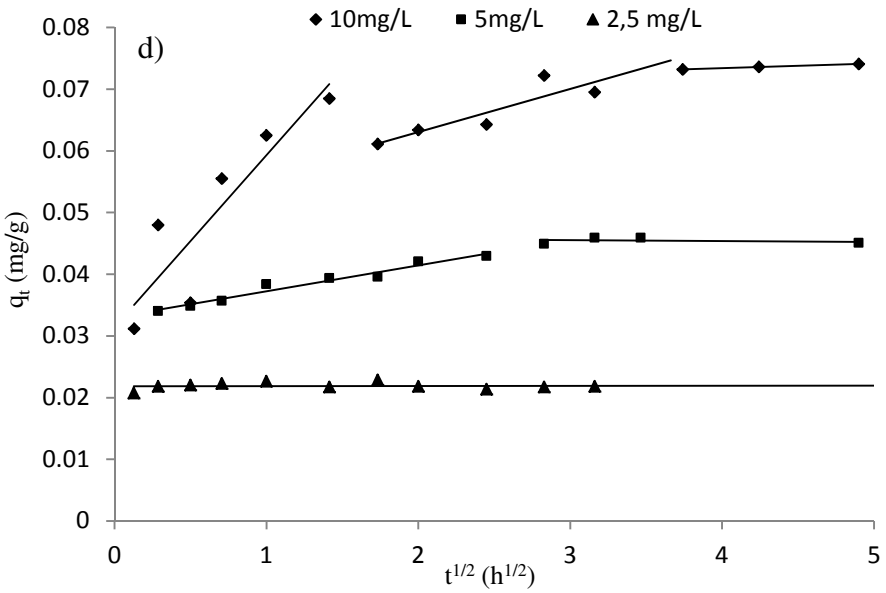

Figure 9. Kinetic model analyses for the phosphate adsorption onto shale in the solution of different initial concentrations (2.5 mg P/L, 5 mg P/L and 10 mg P/L) (a) pseudo-first-order model, (b) pseudo-second-order model (c) Elovich model and (d) intra-particle diffusion model.

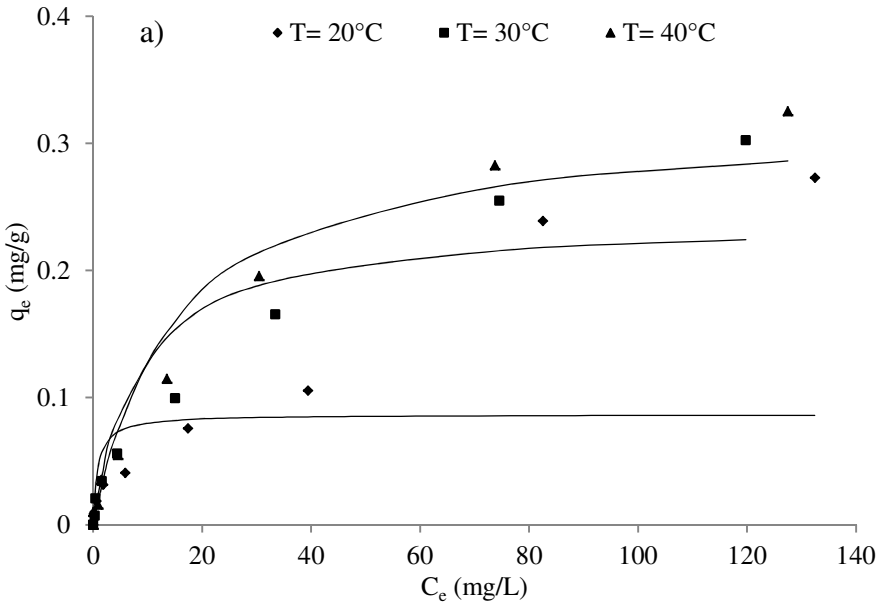

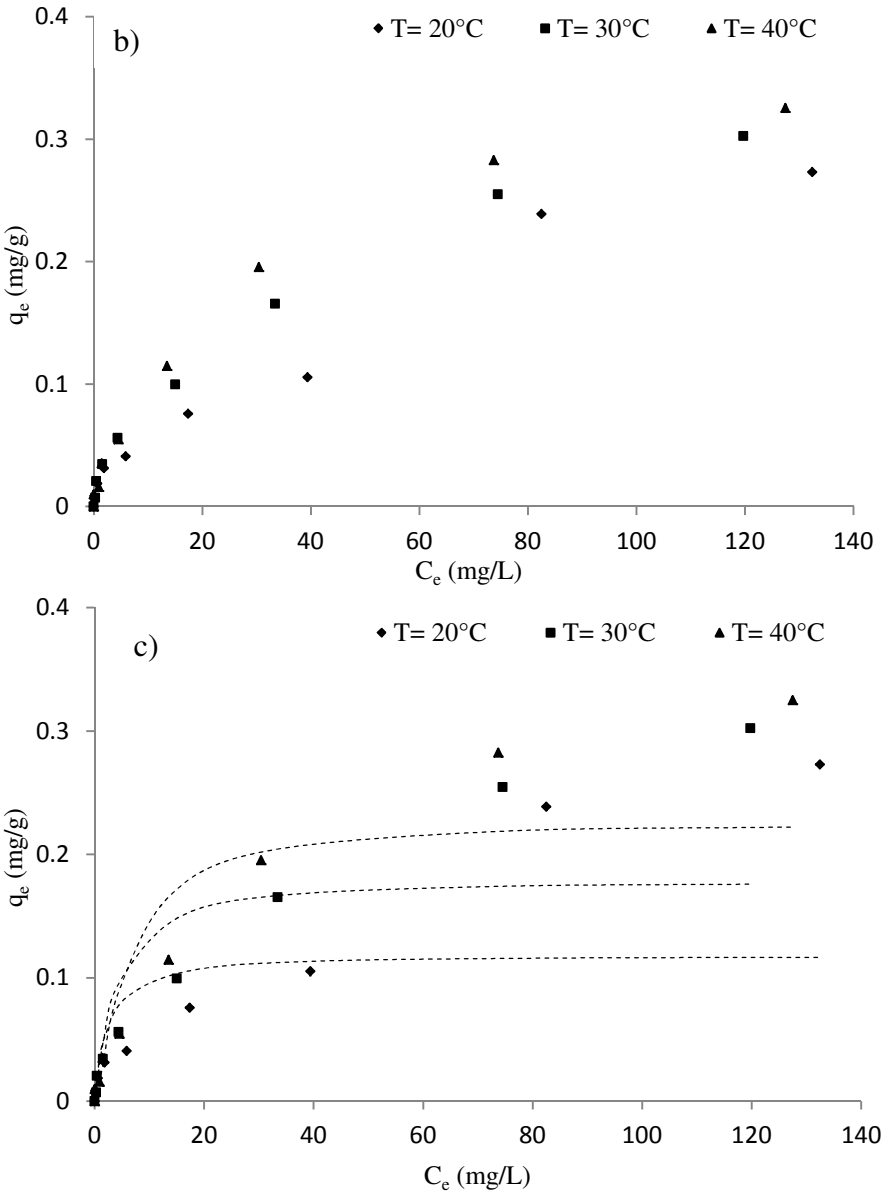

Figure 10. ——Langmuir (a) ·····Freundlich (b) and – – – Dubinin-Radushkevich (c) adsorption isotherms of phosphate onto shale.

Table 5. Isotherms models parameters obtained from model fitting to experimental data.

Temp °C	$q_{m,exp}$ (mg/g)	Langmuir			Freundlich			Dubinin-Radushkevich.			
		$q_{m\,L}$ (mg/g)	k_L (L/mg)	R	K_F	nf	R	$q_{m\,D\text{-}R}$ (mg/g)	β (mol^2/kJ^2)	E (KJ/mol)	R
20	0.273	0.067	1.18	0.960	$22.09.10^{-3}$	2.07	0.989	0.12	0.016	5.52	0.874
30	0.30	0.25	0.12	0.946	$22.42.10^{-3}$	1.78	0.983	0.18	0.024	4.55	0.949
40	0.32	0.30	0.07	0.979	$22.71.10^{-3}$	1.70	0.989	0.25	0.036	3.72	0.972

Table 6. Chi-square (χ^2) analysis values

Temp °C	Langmuir	Freundlich	Dubinin-Radushkevich.
20	0.30	0.03	0.38
30	0.07	0.01	0.17
40	0.02	0.03	0.09

Table 7. Adsorption capacities of different adsorbents for phosphate

Adsorbents	q_e (mg/g)	References
Limestone	0.682	Drizo *et al.* (1999)
Dolomite	0.168	Prochaska & Zouboulis (2006)
Ochre	0.026	Heal *et al.* (2003, 2005)
Soils, Sands, Fly ash, Blast furnace slag	0.29-0.97	Xu *et al.* (2006)

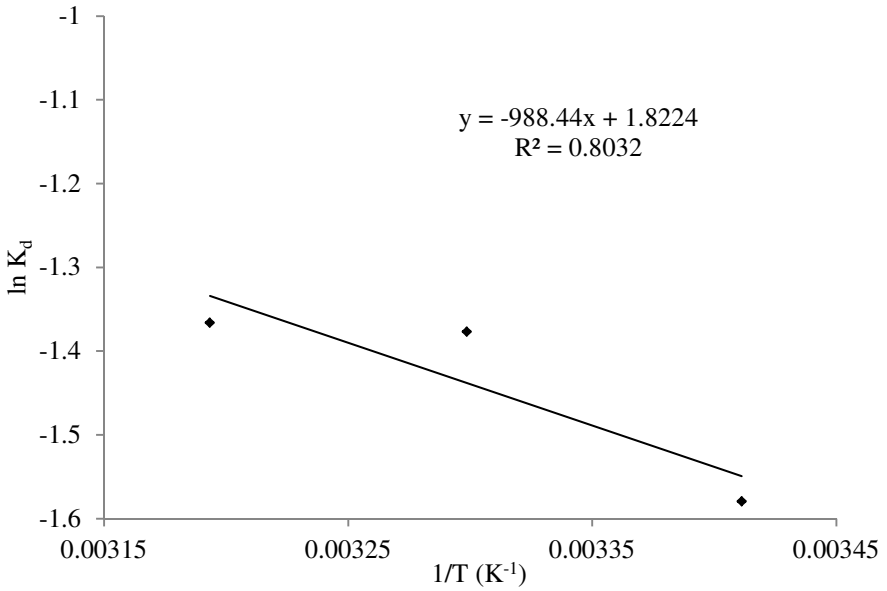

Figure 11. Thermodynamic analysis for phosphate adsorption to shale

Table 8. Thermodynamic parameters for phosphate adsorption to shale

Temp. (°C)	ΔG (KJ/mol)	ΔH (KJ/mol)	ΔS (KJ/mol)
20	3.82		
30	3.67	8.22	0.015
40	3.52		